

# Ultra-Wideband Terahertz Absorption Using Dielectric Circular Truncated Cones

Volume 11, Number 5, October 2019

Longfang Ye

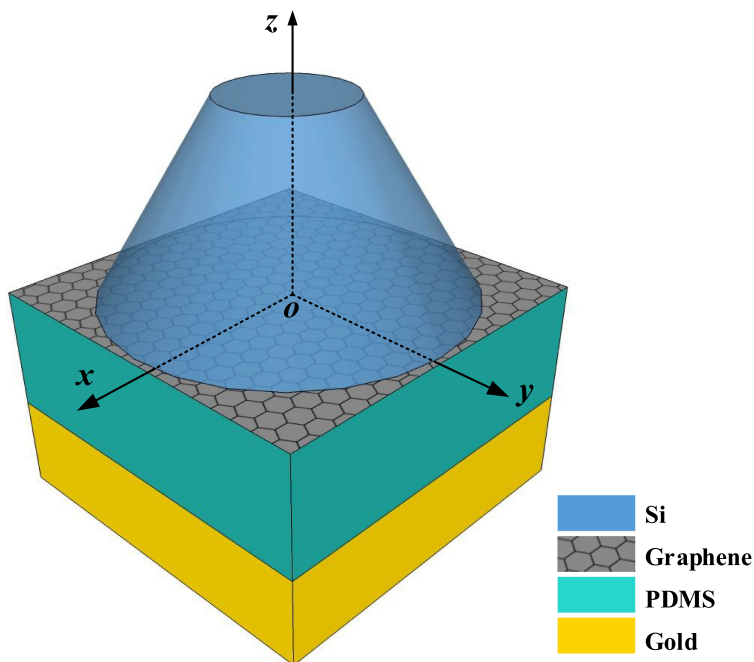
Xin Chen

Fang Zeng

Jianliang Zhuo

Fei Shen

Qing Huo Liu, *Fellow, IEEE*



DOI: 10.1109/JPHOT.2019.2934653

# Ultra-Wideband Terahertz Absorption Using Dielectric Circular Truncated Cones

Longfang Ye<sup>1,2</sup>, Xin Chen,<sup>3</sup> Fang Zeng,<sup>1</sup> Jianliang Zhuo,<sup>1</sup>  
Fei Shen,<sup>4</sup> and Qing Huo Liu<sup>1,5</sup> *Fellow, IEEE*

<sup>1</sup>Institute of Electromagnetics and Acoustics, and Department of Electronic Science, Xiamen University, Xiamen 361005, China

<sup>2</sup>Shenzhen Research Institute of Xiamen University, Shenzhen 518057, China

<sup>3</sup>China Ship Development and Design Center, Wuhan 430064, China

<sup>4</sup>School of Electrical Engineering & Intelligentization, Dongguan University of Technology, Dongguan 523808, China

<sup>5</sup>Department of Electrical and Computer Engineering, Duke University, Durham, NC 27708 USA

DOI:10.1109/JPHOT.2019.2934653

This work is licensed under a Creative Commons Attribution 4.0 License. For more information, see <https://creativecommons.org/licenses/by/4.0/>

Manuscript received July 8, 2019; revised July 30, 2019; accepted August 7, 2019. Date of publication August 12, 2019; date of current version August 23, 2019. This work was supported in part by the National Natural Science Foundation of China under Grant 61601393 and in part by the Shenzhen Science and Technology Projects under Grant JCYJ20180306172733197. Corresponding authors: Longfang Ye; Fei Shen (e-mail: lfye@xmu.edu.cn; shenfei@dgut.edu.cn).

**Abstract:** We numerically demonstrate an ultra-wideband terahertz absorber using dielectric circular truncated cones on a non-structured graphene layer supported by a dielectric spacer on a metal reflector in the bottom. The absorber has an ultra-wideband absorption bandwidth from 0.34 to more than 10 THz with an average absorbance of 95.88% and a relative bandwidth of 186% because of the continuous multimode Fabry-Perot (FP) resonances. The absorber also possesses excellent absorption characteristics with polarization independence under normal incidence and angular stability up to 60°. The proposed ultra-wideband absorber may have promising applications in terahertz trapping, imaging, and detecting.

**Index Terms:** Terahertz, ultra-wideband, absorption.

## 1. Introduction

Terahertz technology has attracted extensive attention in recent years [1]. As one of the key devices in terahertz region, terahertz absorbers have great applications in terahertz imaging, thermal detectors, and communication [2]–[5]. Recently, various terahertz absorbers with different structures including electric ring resonators (ERRs) [6], [7], patterned graphene absorbers [8]–[13], and all dielectric absorbers [14], [15] have been investigated. However, most of these absorbers are operating in a single-band, dual-band, or multi-band with limited absorption bandwidth.

In order to increase the terahertz absorption bandwidth, multi-resonator and multi-layer structures have been designed by introducing more resonances in the absorbers [11]–[13], [16]–[22]. For example, Ye *et al.* demonstrated a hybrid-patterned graphene metasurface based broadband absorber with a 90% absorbance bandwidth from 1.38 to 3.4 THz and a corresponding relative bandwidth of 84.5% [13]. Xu *et al.* proposed an ultra-broadband absorber based on multilayer-graphene with an absorption band ranging from 3 to 7.8 THz and a relative bandwidth of 89% [16]. Kenney *et al.* proposed a fractal crosses supercell structured THz absorber with an average absorbance of 80% from 2.82 to 5.15 THz and a relative bandwidth of 58% [17]. However,

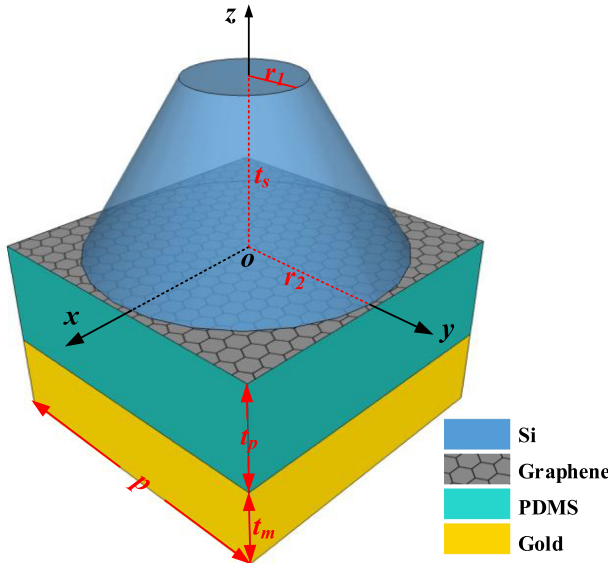


Fig. 1. Schematic of the unit cell of the proposed ultra-wideband absorber, where  $p = 170 \mu\text{m}$ ,  $t_m = 1 \mu\text{m}$ ,  $t_p = 25 \mu\text{m}$ ,  $t_s = 110 \mu\text{m}$ ,  $r_1 = 45 \mu\text{m}$  and  $r_2 = 84 \mu\text{m}$ .

such broadband absorbers with multi-layer and multi-resonator structures still suffer from some drawbacks such as the increased fabrication complexity, multi-graphene gating problem, complicate super unit cell structure. To simplify the structure, Yang *et al.* proposed a simple absorber based on non-structured graphene and elliptic dielectric cylinders showing the 90% absorbance bandwidth ranging from 1.57 to 3.07 THz and a relative bandwidth of 65% [18]. It is clear that the relative bandwidths of most recently designed broadband absorbers are still very limited, usually less than 100%. How to achieve a high-performance terahertz absorber with ultra-wideband absorption and simple structure simultaneously is of great significance in various promising terahertz applications.

In this paper, we propose a novel ultra-wideband terahertz absorber based on dielectric circular truncated cones on a non-structured graphene layer supported by a dielectric spacer on a metal reflector in the bottom. To demonstrate the characteristics of the proposed ultra-wideband absorber, the absorbance spectra, electric field distributions, polarization dependence, and angular stability are investigated and discussed. The simulation results reveal that the proposed absorber can absorb the incident terahertz waves ranging from 0.34 to 10 THz with an average absorbance of 95.88%. The relative terahertz absorption bandwidth is over 186%, which to the best of our knowledge is the highest value compared to the recently reported broadband absorbers. The ultra-wideband absorption characteristic of the proposed absorber is mainly attributed to the continuous multimode FP resonances, which is fundamentally different from the localized surface plasmon resonance of the patterned graphene in the reported broadband graphene absorbers [8]–[13].

## 2. Absorber Structure

As shown in Fig. 1, the schematic of ultra-wideband absorber unit cell is composed of a multi-layer structure consisting of a silicon (Si) right circular truncated cone, a continuous single-layer graphene, a polydimethylsiloxane (PDMS) spacer, and a gold (Au) reflector from top to the bottom. The thicknesses of gold, PDMS, and Si layers are set as  $t_m = 1 \mu\text{m}$ ,  $t_p = 25 \mu\text{m}$  and  $t_s = 110 \mu\text{m}$ , respectively. The period of the unit cell  $p = 170 \mu\text{m}$  in both  $x$  and  $y$  directions, the Si circular truncated cone with a top radius  $r_1 = 45 \mu\text{m}$  and a bottom radius  $r_2 = 84 \mu\text{m}$ . Based on the experimentally measured data in [23], we set the dielectric constants of Si as  $\epsilon_1 = 11.65$  and  $\tan \delta_1 = 0.174$ ,

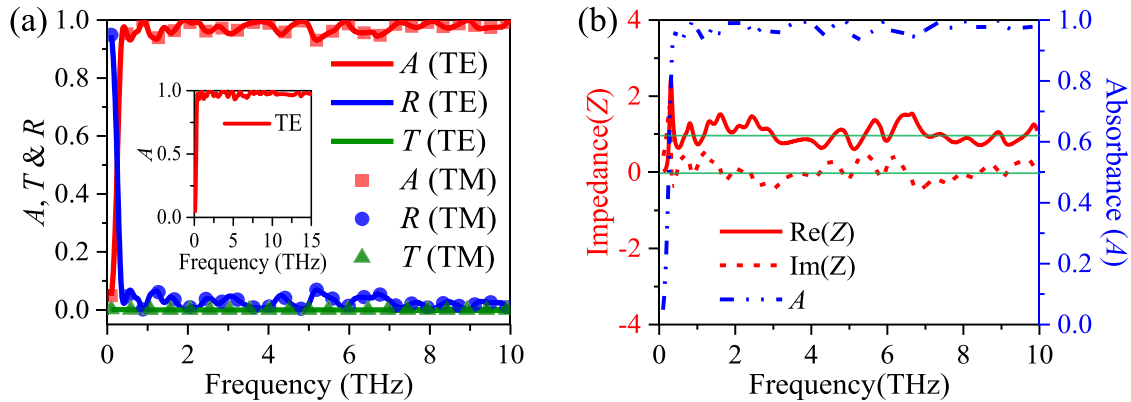


Fig. 2. (a) Simulated absorbance ( $A$ ), reflectance ( $R$ ), and transmission ( $T$ ), of the proposed absorbers for both TE and TM polarizations under normal incidence; (b) Extracted normalized effective impedance ( $Z$ ) of the proposed absorbers.

and that of PDMS as  $\varepsilon_2 = 1.72$  and  $\tan \delta_2 = 0.15$  in our simulation. The gold is modeled as a dispersive medium using the Drude model [24],  $\varepsilon(\omega) = \varepsilon_\infty - \omega_p^2/(\omega^2 + i\omega_\gamma)$ , where  $\varepsilon_\infty = 1$ ,  $\omega_p = 1$ ,  $7.25 \times 10^4 \text{ cm}^{-1}$  is the plasma frequency, and  $\omega_\gamma = 1.45 \times 10^2 \text{ cm}^{-1}$ , respectively. In the terahertz region, the graphene can be modeled as a 2D surface conductivity ( $\sigma_g$ ) layer by the Kubo formula [25]–[27]. In the finite element method based numerical simulation, two Floquet ports are employed to model the incident and output polarized waves in z-direction of the proposed unit cell with the periodic boundaries in both x and y directions. The absorbance ( $A$ ) of the absorber is obtained by  $A = 1 - R - T$ , where the reflectance  $R = |S_{11}|^2$  and transmission  $T = |S_{21}|^2$ , respectively.

### 3. Results and Discussion

We first demonstrate the terahertz absorption properties for the TE and TM polarizations of the proposed ultra-wideband absorber under normal incidence. We set the initial graphene relaxation time and Fermi level as  $\tau = 0.1 \text{ ps}$  and  $\mu_c = 0.7 \text{ eV}$ , respectively. The absorbance  $A$ , reflection  $R$ , and transmission  $T$  of the absorber are shown in Fig. 2(a). Obviously, because of the axisymmetric structure, the absorbance spectra for both polarizations of the proposed absorber are completely coincident, showing excellent polarization-insensitivity. It is found that the absorber has an average absorbance of 95.88% in an ultra-wideband between 0.34 to 10 THz. The corresponding relative bandwidth (the absolute bandwidth over the central absorption frequency) of this absorber is 186.8%. And the high absorbance characteristics can maintain to even higher frequency up to 15 THz, as shown in the inset of Fig. 2(a). Fig. 2(b) shows the extracted normalized effective impedance ( $Z$ ) of the absorber using the effective medium theory [28]. The results indicate that the real part  $\text{Re}(Z)$  is around 1 (red solid curve) and the imaginary part  $\text{Im}(Z)$  is around 0 (red dashed curve) in the absorbance frequency band ranging from 0.34 to 10 THz, implying that the impedance of the absorber nearly matches the free space. Therefore, the proposed absorber can achieve ultra-wideband high absorbance.

Here, we introduce the interference theory to interpret the absorption phenomenon [29]. In the interference model, we decoupled the absorber into two tuned interfaces, the top of Si circular truncated cones and the gold reflector. As shown in Fig. 3(a), the gold reflection coefficient of gold is  $-1$  and the total reflection of the absorber is calculated by  $\tilde{r} = \tilde{r}_{12} - \frac{\tilde{t}_{12}\tilde{r}_{21}e^{i2\tilde{\beta}}}{1+\tilde{r}_{21}e^{i2\tilde{\beta}}}$ , where the reflection coefficients  $\tilde{r}_{12} = r_{12}e^{i\phi_{12}}$ ,  $\tilde{r}_{21} = r_{21}e^{i\phi_{21}}$ , the transmission coefficients  $\tilde{t}_{12} = t_{12}e^{i\theta_{12}}$ ,  $\tilde{t}_{21} = t_{21}e^{i\theta_{21}}$ , the transmission phase  $\tilde{\beta} = \sqrt{\varepsilon_d}k_0h_2$  and  $k_0$  is the free space wavenumber, respectively. We obtain the reflection and transmission coefficients at the air-dielectric interface by simulating the proposed absorber unit cell without gold reflector plate, as shown in Figs. 3(a) and 3(b). Then, we calculate

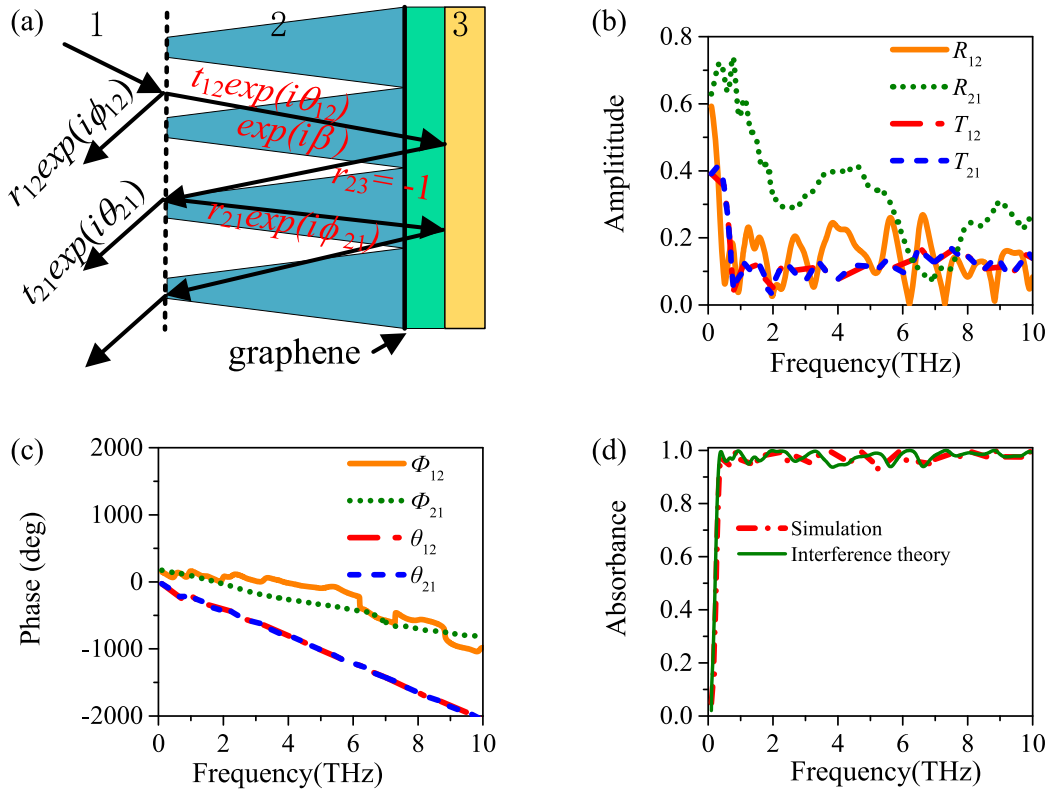


Fig. 3. (a) Interference model of the proposed absorber. (b) and (c) are the amplitude and phase of the reflection and transmission coefficients for the absorber unit cell without gold reflector plate, respectively. (d) Comparison of the interference theory and simulation absorption spectra of the proposed absorber.

the absorbance spectrum of the proposed absorber using  $A(\omega) = 1 - |\tilde{r}(\omega)|^2$  as shown in Fig. 3(c), which is in good agreement with simulation result.

To further study the mechanism of the ultra-wideband terahertz absorption of the absorber, we investigate the electric field distributions of the absorber at 12 different frequencies from 0.1 to 10 THz under normal TE polarized terahertz incidence. In this absorber design, graphene is considered as a partial reflector with damping. The Fabry-Pérot cavity of the proposed absorber is formed between the top of the Si circular truncated cones and the gold reflector at the bottom, which determines the terahertz absorption performance. Fig. 4 shows the side-views of the electric field distributions on  $x$ - $z$  plane. It is obvious that stronger Fabry-Perot (FP) resonances are observed at different frequencies with a high absorption more than 90% ranging from 1 to 10 THz, while much smaller electric field distribution is observed at 0.2 THz with the corresponding absorbance of 29% and extremely weak electric field distribution is observed at 0.1 THz with the corresponding absorbance of 5%. Figs. 4(c)–(l) clearly show that the electric field patterns are related to the different orders (or absorption frequency) of the FP resonances in the Si circular truncated cone. For example, it is the first order FP resonance at 1 THz, the second order FP resonance at 2 THz, and the order of FP resonance increases with the frequency increasing from 1 to 10 THz. The ultra-wideband absorption characteristic of the proposed absorber is attributed to the continuous multimode FP resonances.

In this absorber design, the total dielectric spacer thickness of the FP cavity plays a major role in determining the lowest absorbance frequency and bandwidth of the absorber. Figs. 5(a) and 5(b) show the absorbance spectra of the proposed absorber with different dielectric spacer thickness (Si layer  $t_s$  and PDMS layer  $t_p$ ) for both TE and TM polarizations under normal incidence,

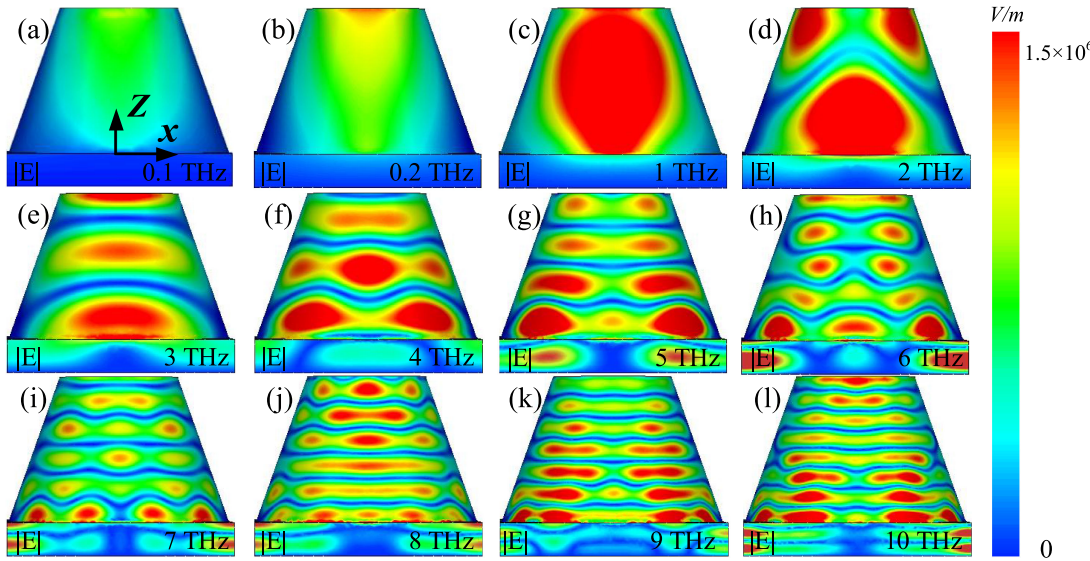


Fig. 4. Simulated side-views of the electric field distributions for TE polarization of the proposed absorber under normal incidence at (a) 0.1 THz, (b) 0.2 THz, (c) 1 THz, (d) 2 THz, (e) 3 THz, (f) 4 THz, (g) 5 THz, (h) 6 THz, (i) 7 THz, (j) 8 THz, (k) 9 THz, (l) 10 THz, respectively.

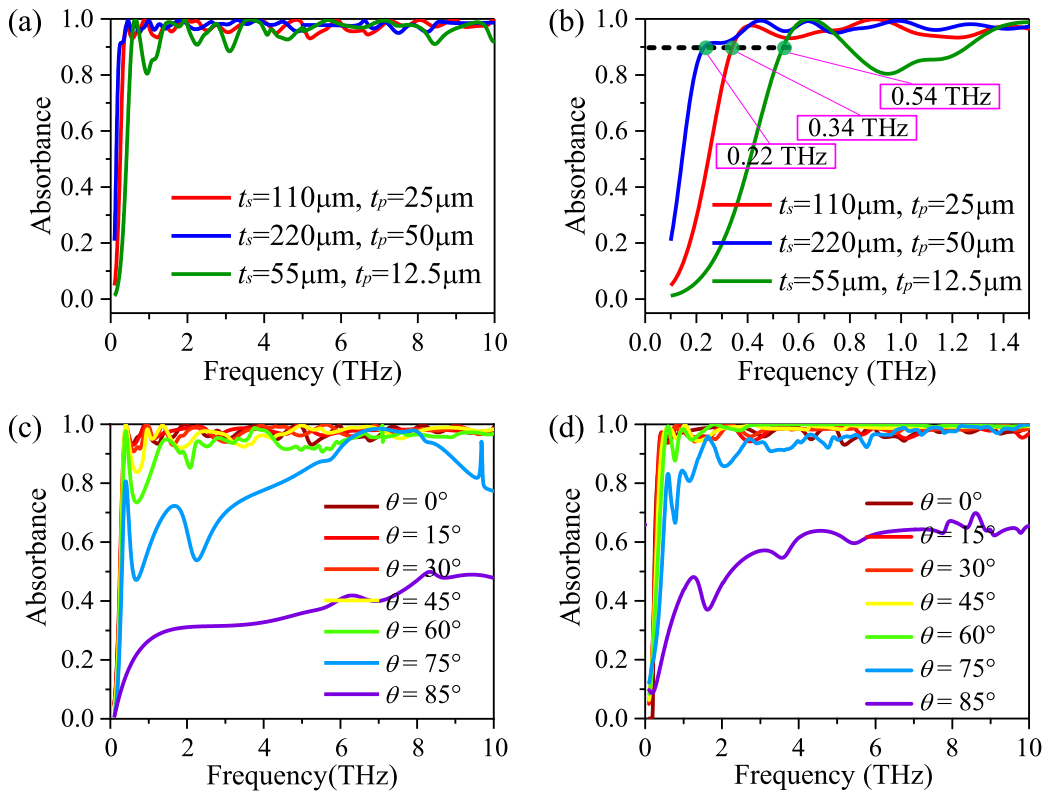


Fig. 5. (a) and (b) are the absorbance spectra of the proposed absorber with different dielectric spacer thickness ( $t_s + t_p$ ) for both TE and TM polarizations under normal incidence, where (a) focused on 0–10 THz and (b) focused on 0–1.5 THz. (c) and (d) are the absorbance spectra of the proposed absorber for the TE polarization and TM polarization under different terahertz incident angles of  $0^\circ$ ,  $15^\circ$ ,  $30^\circ$ ,  $45^\circ$ ,  $60^\circ$ ,  $75^\circ$ , and  $85^\circ$ , respectively.

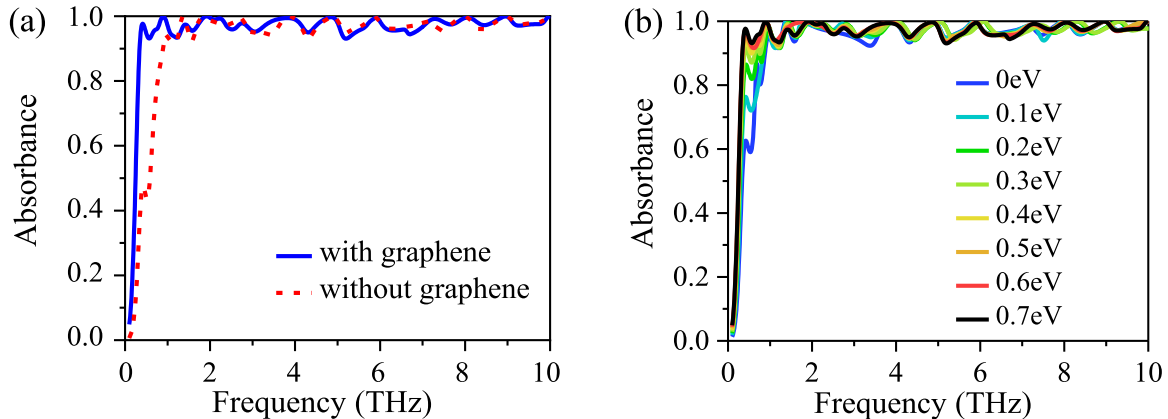


Fig. 6. (a) Absorbance spectra with and without graphene. (b) Absorbance with different Fermi levels from 0 eV to 0.7 eV.

where (a) focused on 0–10 THz and (b) focused on 0–1.5 THz. It is clear that the lowest absorbance frequency decreases and the bandwidth increases as the total dielectric spacer thickness increases. Furthermore, the dependence of the absorbance spectra on the angle of incidence of the proposed absorber under TE and TM polarizations is studied. As shown in Fig. 5(c), we observe that the average absorbance maintains over 90% with only small ripples in the absorption band under a wide angle of incidence ranging from 0° to 60° for TE polarization, while the absorbance significantly decreases to lower than 70% when the incident angle is larger than 75°. Fig. 5(d) shows that the absorbance spectra for the TM polarization are also insensitive to the incident angle up to 60° in the whole frequency band and has a drastic decline as the incident angle increase to 75°. Therefore, the proposed absorber exhibits excellent angular stability for both polarizations even at a large angle of 60°, which is very promising for various terahertz application scenarios.

In addition, we study the effects of graphene on the absorbance of the proposed terahertz absorber. The absorbance spectra of the absorber with and without graphene are compared in Fig. 6(a). We find that the 90% absorption bandwidth of the proposed absorber with graphene is wider than that of the absorber without graphene. By introducing the graphene layer in the absorber design, the low-frequency end of the 90% absorbance is greatly extended from 0.88 to 0.33 THz. We calculated the average absorbance of the absorber with or without graphene between 0.9 and 10 THz. We also find that the average absorbance of the absorber with graphene is 97.42%, which is slightly higher than the average absorbance of 97.21% for the absorber without graphene sheet. Fig. 6(b) shows the absorbance spectra as a function of the graphene Fermi level ranging from 0 to 0.7 eV. It is found that the absorbance is enhanced as the Fermi level increases, especially at the frequency region below 0.9 THz. Therefore, the graphene plays a key role in enhancing the absorber's absorbance in the low-frequency region below 0.9 THz.

#### 4. Conclusion

We have demonstrated a high-performance ultra-wideband terahertz absorber based on the dielectric circular truncated cones and a single-layer graphene. The absorber has an ultra-wideband absorption from 0.34 to more than 10 THz with a high average absorbance of 95.88% and a fractional bandwidth of 186%. The ultra-wideband absorption is attributed to the continuous multimode FP resonance in the dielectric truncated cones. The results show that the absorber has absolute independence of polarizations under normal incidence due to the symmetric structure and excellent angular stability with average absorbance of 90% up to 60° for both TE and TM-polarization incident terahertz waves. The proposed absorber with both simple configuration and excellent ultra-wideband high absorbance may have extensive applications in terahertz trapping, imaging, and detecting.

## References

- [1] M. Tonouchi, "Cutting-edge terahertz technology," *Nature Photon.*, vol. 1, pp. 97–105, 2007.
- [2] J. Liu, L. Fan, J. Ku, and L. Mao, "Absorber: A novel terahertz sensor in the application of substance identification," *Opt. Quantum Electron.*, vol. 48, 2016, Art. no. 80.
- [3] N. I. Landy, C. M. Bingham, T. Bingham, N. Jokerst, D. R. Smith, and W. J. Padilla, "Design, theory, and measurement of a polarization insensitive absorber for terahertz imaging," *Phys. Rev. B*, vol. 79, 2009, Art. no. 125104.
- [4] I. Escoria, J. Grant, J. Gough, and D. R. S. Cumming, "Uncooled CMOS terahertz imager using a metamaterial absorber and PN diode," *Opt. Lett.*, vol. 41, pp. 3261–3264, 2016.
- [5] L. Vicarelli, M. S. Vitiello, D. Coquillat, A. Lombardo, A. C. Ferrari, and W. Knap, "Graphene field-effect transistors as room-temperature terahertz detectors," *Nature Mater.*, vol. 11, pp. 865–871, 2012.
- [6] H. Tao *et al.*, "Highly flexible wide angle of incidence terahertz metamaterial absorber: Design, fabrication, and characterization," *Phys. Rev. B*, vol. 78, 2008, Art. no. 241103.
- [7] H. Tao, N. I. Landy, C. M. Bingham, X. Zhang, R. D. Averitt, and W. J. Padilla, "A metamaterial absorber for the terahertz regime: Design, fabrication and characterization," *Opt. Exp.*, vol. 16, pp. 7181–7188, 2008.
- [8] S. Thongrattanasiri, F. H. Koppens, and F. J. G. De Abajo, "Complete optical absorption in periodically patterned graphene," *Phys. Rev. Lett.*, vol. 108, 2012, Art. no. 047401.
- [9] L. Ye, F. Zeng, Y. Zhang, X. Xu, X. Yang, and Q. H. Liu, "Frequency-reconfigurable wide-angle terahertz absorbers using single- and double-layer decussate graphene ribbon arrays," *Nanomaterials*, vol. 8, no. 10, 2018, Art. no. 834.
- [10] L. Ye, F. Zeng, Y. Zhang, and Q. H. Liu, "Composite graphene-metal microstructures for enhanced multiband absorption covering the entire terahertz range," *Carbon*, vol. 148, pp. 317–325, 2019.
- [11] L. Ye *et al.*, "Broadband absorber with periodically sinusoidally-patterned graphene layer in terahertz range," *Opt. Exp.*, vol. 25, no. 10, pp. 11223–11232, 2017.
- [12] L. Ye, X. Chen, J. Zhuo, F. Han, and Q. H. Liu, "Actively tunable broadband terahertz absorption using periodically square-patterned graphene," *Appl. Phys. Exp.*, vol. 11, no. 10, 2018, Art. no. 102201.
- [13] L. Ye, X. Chen, G. Cai, J. Zhu, N. Liu, and Q. H. Liu, "Electrically tunable broadband terahertz absorption with hybrid-patterned graphene metasurfaces," *Nanomaterials*, vol. 8, no. 8, 2018, Art. no. 562.
- [14] K. Fan, J. Y. Suen, X. Liu, and W. J. Padilla, "All-dielectric metasurface absorbers for uncooled terahertz imaging," *Optica*, vol. 4, 2017, Art. no. 601.
- [15] M. A Cole, D. A Powell, and I. V Shadrivov, "Strong terahertz absorption in all-dielectric Huygens' metasurfaces," *Nanotechnology*, vol. 27, 2016, Art. no. 424003.
- [16] Z. Xu *et al.*, "Design of a tunable ultra-broadband terahertz absorber based on multiple layers of graphene ribbons," *Nanoscale Res. Lett.*, vol. 13, 2018, Art. no. 143.
- [17] M. Kenney, J. Grant, Y. D. Shah, I. E. Carranza, M. Humphreys, and D. R. S. Cumming, "Octave-spanning broadband absorption of terahertz light using metasurface fractal-cross absorbers," *ACS Photonics*, vol. 4, pp. 2604–2612, 2017.
- [18] J. Yang *et al.*, "Broadband terahertz absorber based on multi-band continuous plasmon resonances in geometrically gradient dielectric loaded graphene plasmon structure," *Sci. Rep.*, vol. 8, 2018, Art. no. 3239.
- [19] S. Yi, M. Zhou, X. Shi, Q. Gan, J. Zi, and Z. Yu, "A multiple-resonator approach for broadband light absorption in a single layer of nanostructured graphene," *Opt. Exp.*, vol. 23, pp. 10081–10090, 2015.
- [20] F. Gao *et al.*, "Broadband wave absorption in single-layered and nonstructured graphene based on far-field interaction effect," *Opt. Exp.*, vol. 25, pp. 9579–9586, 2017.
- [21] M. Amin, M. Farhat, and H. Bagci, "An ultra-broadband multilayered graphene absorber," *Opt. Exp.*, vol. 21, pp. 29938–29948, 2013.
- [22] S. He and T. Chen, "Broadband THz absorbers with graphene-based anisotropic metamaterial films," *IEEE Trans. Terahertz Sci. Technol.*, vol. 3, no. 6, pp. 757–763, Nov. 2013.
- [23] A. Cardin, K. Fan, and W. Padilla, "Role of loss in all-dielectric metasurfaces," *Opt. Exp.*, vol. 26, pp. 17669–17679, 2018.
- [24] M. A. Ordal *et al.*, "Optical properties of the metals Al, Co, Cu, Au, Fe, Pb, Ni, Pd, Pt, Ag, Ti, and W in the infrared and far infrared," *Appl. Opt.*, vol. 22, pp. 1099–1120, 1983.
- [25] V. P. Gusynin, S. G. Sharapov, and J. P. Carbotte, "Magneto-optical conductivity in graphene," *J. Phys. Condens. Mater.*, vol. 19, 2006, Art. no. 026222.
- [26] G. W. Hanson, "Dyadic Green's functions and guided surface waves for a surface conductivity model of graphene," *J. Appl. Phys.*, vol. 103, 2008, Art. no. 064302.
- [27] G. W. Hanson, "Dyadic Green's functions for an anisotropic, non-local model of biased graphene," *IEEE Trans. Antennas Propag.*, vol. 56, pp. 747–757, Mar. 2008.
- [28] D. R. Smith, D. C. Vier, T. Koschny, and C. M. Soukoulis, "Electromagnetic parameter retrieval from inhomogeneous metamaterials," *Phys. Rev. E*, vol. 71, 2005, Art. no. 036617.
- [29] T. Chen, "Interference theory of metamaterial perfect absorbers," *Opt. Exp.*, vol. 20, no. 7, pp. 7165–7172, 2012.